International Journal of Scientific Engineering and Science
Volume 3, Issue 9, pp. 15-19, 2019. ISSN (Online): 2456-7361

Facile Fabrication and Characterization of Free-Hole Perovskite Solar Cell Based on Carbon Electrode

Hassan Elshimy*, Tamer Abdallah, Ali Abou Shama
Physics Department, Faculty of Science, Ain Shams University, Cairo, Egypt

Abstract— *Free-hole perovskite solar cell without precious metals electrode are the chief toward large scale and low cost production of perovskite solar cells, and thus commercialization. In this study, TiO2/CH3NH3PbI3/C devices were fabricated in air using carbon as a counter electrode with the aid of the facile doctor blade technique, which simplifies the processing and lowers the threshold of fabrication process. Three different approaches were used to deposit the carbon paste and finalize the perovskite devices. The structure and microstructural of the perovskite layers were studied using XRD and FTIR. The photovoltaic performance were studied, for the devices fabricated by different method, and it was found that, the way to deposit the carbon paste has a great influence on the power conversion efficiencies and devices reproducibility.*

Keywords— *Carbon, Perovskite, Solar cell, XRD.*

I. INTRODUCTION

Organo-metal halide perovskites have attracted great attention from scientists all around the world because of their tunable band gap, large absorption coefficient, high charge carrier mobility, and long electron−hole diffusion [1-7]. These properties made such materials candidate as an alternative to silicon for making inexpensive and efficient solar cells [8-9].

A typical perovskite solar cell (PSCs) consists of electron transport layer (ETL), perovskite layer, hole transport material (HTM) and noble metal as a counter electrode [10, 11]. The most common ETL are TiO2 and ZnO which are environmentally friendly nature, stable and low cost materials besides their facile syntheses [12-14]. Unfortunately, the organic hole transporter materials (such as spiro-OMeTAD or PTAA) are expensive and unstable. [15, 16]. In addition, the noble metals such as Au or Ag electrode are also costly. Besides, the high-energy-consumption vacuum evaporation method of preparing such metals restrains its marketing as well. Therefore, the replacement of such materials are urgently required by developing an alternative materials that process the same function but are cheap, earth-abundant, environmentally friendly and easily processable. To meet with the demand of simple and low-cost perovskite solar cells, some inorganic hole-transport materials [17, 18] have been developed such as CuSCN and CuI.

Through the unremitting endeavor of many research groups, carbon materials as the cost-efficient choice of counter electrodes have been introduced. As is well known, graphitic carbon, with most of the abovementioned sought-after characteristics, has suitable Fermi level (work function of around 5.0 eV), meaning that its Fermi level is only slightly higher than the valence band edge of the perovskites. [11, 19, 20]. This energy band alignment probably permits the graphitic carbon to efficiently work as a hole transport layer, in addition to a counter electrode, which is an imperative step toward the low cost solar cell [11, 19, 21, 22]. The deposition of carbon electrode plays an important role in the performance of PSCs.

Here, we fabricated a perovskite solar cells with structure FTO/TiO2/CH3NH3PbI3/C. The devices were fabricated using three different methods of depositing carbon paste by doctor blade technique. The photovoltaic parameters were studied in order to achieve the best and optimum method for carbon deposition.

II. MATERIALS AND METHODS

A. Device fabrication

FTO glasses were etched (using Zinc powder and HCl) then cleaned in an ultrasonic bath containing isopropanol and deionized water for 10 min. For the TiO2 layer, a solution consisting of 175 mL of TTIP in 1.25 mL of isopropanol was added to a solution of 17.5 mL of HCl in 1.25 mL of isopropanol and spun coated on FTO substrates at 3500 rpm for 30 s [23]. Subsequently, the films were annealed in air at 450 °C for 45 min. In the three different methods, CH3NH3PbI3 was formed using two-step spin dipping procedure [7]. PbI2 solution was prepared by dissolving 462 mg PbI2 in 1 ml N,N-dimethylformamide (DMF) under stirring at 70 °C. PbI2 solution was spin-coated on the TiO2 film at 6,000 r.p.m. for 30 s, subsequently, the films were dried at 70 °C for 30 min, and then allowed to cool to room temperature. The formation of the perovskite layer and the deposition of carbon paste were provided by three different methods:

In method 1 (Direct deposition), after cooling PbI2 film to room temperature, the film was dipped in a solution of CH3NH3I in 2-propanol (10 mg / ml) for 20 s. The color of the film immediately changes from yellow to dark brown, indicating the formation of CH3NH3PbI3. The film then rinsed with 2-propanol, to remove ammonium salt residues in the perovskite film, then annealed at 100 °C for 30 min on a preheated hot plate at ambient atmosphere.

Finally, once the perovskite film cooled down to room temperature, the commercial carbon paste was deposited on the film by doctor–blading technique, and dried at 100 °C for 30 min. All these procedures were carried out on naturally ambient atmosphere, Fig. 1

International Journal of Scientific Engineering and Science
Volume 3, Issue 9, pp. 15-19, 2019. ISSN (Online): 2456-7361

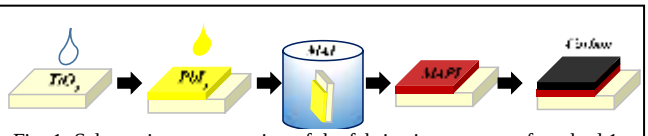

Fig. 1. Schematic representation of the fabrication process of method 1 (By direct depositing C paste on CH3NH3PbI3 Film)

In method 2, after cooling PbI2 film to room temperature, a carbon paste was deposited by doctor bladed on the top of the PbI2 layer and dried at 100 °C for 30 min and then allowed to cool to room temperature. Finally, the film was dipped in a solution of CH3NH3I in 2-propanol (10 mg / ml) for 20 s then rinsed with 2-propanol and dried at 100 °C for 30 min in air. In a similar manner, the color changing from yellow to dark brown indicates a perovskite film is generated, demonstrating the completion of the fabrication of devices, Fig. 2.

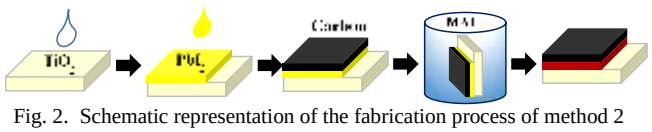

Fig. 2. Schematic representation of the fabrication process of method 2 (By applying C paste on PbI2 film then dipping in CH3NH3I bath)

In method 3 (clamping solar cell), The PbI2 film was soaked into a CH3NH3I bath to get a CH3NH3PbI3 film (The procedures were similar to Method 1). Another Piece of FTO was coated with carbon paste and dried at 100 °C for 30 min. The FTO/C film and the CH3NH3PbI3 film were directly clamped. The FTO/C film then directly clamped to the CH3NH3PbI3 film, completing the device fabrication, Fig. 3.

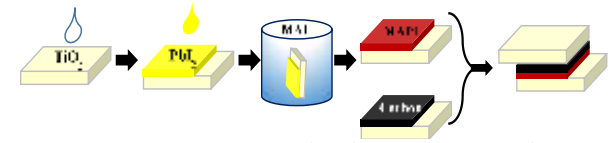

Fig. 3. Schematic representation of the fabrication process of method 3 (Clamping solar cell)

B. Characterization

The investigation of structure and microstructural of perovskite device layers were mainly studied using x-ray diffraction technique. XRD patterns of the different layers were collected using Cu-Kα radiation of Philips diffractometer (X′pert MPD) operating at 40kV and 30 mA. The crystal structure and microstructure were refined applying Rietveld profile method, using MAUD program [24, 25]. LaB6 standard has been used to correct the instrumental broadening.

FT-IR spectroscopy is a power tool for identifying types of chemical bonds in a molecule. The spectroscopic analyses of MAI powder was carried out using FTIR spectrometer (FT/IR-620) in the wave number range of 4000–400 cm-1.

Photovoltaic solar cell measurements were performed using a solar simulator device (Sol3A Class AAA) at AM 1.5 with 1 sun illumination intensity (100 mW/cm² at 25 °C), and current density–voltage (J–V) data were recorded using a source meter unit (Keithley 2400).

III. Results and Discussion

A. Characterization of Perovskite device layers

XRD pattern of TiO2 film deposited via spin coating, Fig. 4, shows two characteristic peaks at 25.35° and 37.8°, which belong to (101) and (004) planes of the Tetragonal anatase TiO_2 phase with lattice parameters a= 3.77 A° and c= 9.51 A°, ICDD no. 01-089-4921. The crystallite sizes of TiO2 particles was estimated using Scherrer formula, given by

$$D = \frac{K\lambda}{\beta \cos\theta},$$

where D is the crystallite size, k is a constant, λ is the x-ray wavelength (0.1540 nm), β is the integral breadth of the diffraction peak. For more realistic calculation, the instrumental broadening was deconvoluted and therefore the calculations estimated an average crystallite size of 8 nm.

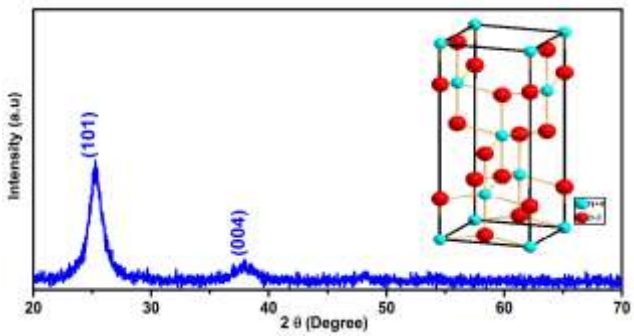

Fig. 4. The XRD pattern of TiO2 thin film. Insert shows the Tetragonal system of the anatase phase

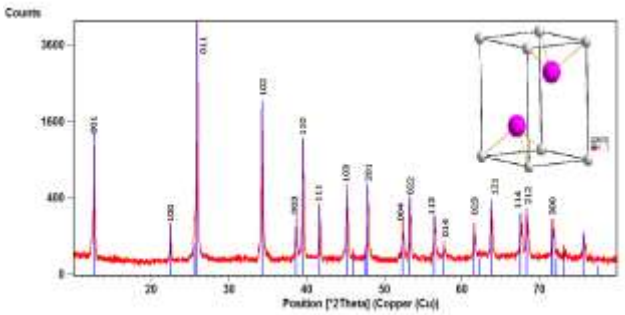

Fig. 5. The XRD pattern of PbI2 powder. Insert shows the Hexagonal system of PbI2 phase

X-ray diffraction patterns of the PbI2 powder is shown in fig. 5. The diffraction peaks obtained at 12.66°, 22.50 °, 25.9 °, 34.25 °, 39.63 °, 39.51 °, 41.65 °, 45.17 °, 47.85 °, 52.34 °, 53.26 °, 56.45 °, 57.67 °, 61.54 °, 63.73 °, 67.51 °, 68.30 °, 71.66 °, 73.12 ° and 75.63 ° are assigned respectively to the planes (001) , (100) , (011) , (102) , (003) , (110) , (111) , (103) , (201) , (004) , (022) , (113) , (014) , (023) , (121) , (114) , (212) , (300) , (031) and (213) of Hexagonal phase PbI2 with the space group of *P-3m1*. No spurious diffractions peaks were observed which indicate the purity of the used PbI2 powder. The lattice parameters and crystallite size of each plane were obtained using Rietveld method with the aid of

International Journal of Scientific Engineering and Science
Volume 3, Issue 9, pp. 15-19, 2019. ISSN (Online): 2456-7361

Maud program. The obtained results, listed in table 1, show a crystallite size dependence on the crystallographic planes.

Table 1: Microstructural parameters obtained from Rietveld analysis

Lattice parameter (A^o)		Crystallite size (nm)				
a	**c**	**001**	**100**	**011**	**012**	**111**
4.557	6.98	556	856	783	688	827

X-ray diffraction pattern of the synthesized methylammonium iodide (MAI) is shown in fig. 6. A strong Bragg reflections at 19.66^o , 19.91^o , 24.54^o , 26.29^o , 29.66^o , 31.64^o , 34.54^o , 34.99^o , 36.39^o , 38.87^o , 40.58^o , 43.8^o and 44.29^o were observed, which corresponding to (002), (101), (110), (102) , (003) , (112), (103), (200), (201), (113), (211), (104) and (212) planes of MAI. XRD Search matching confirms the formation of Tetragonal phase with lattice parameters a= 5.12 A^o and c= 9.00 A^o

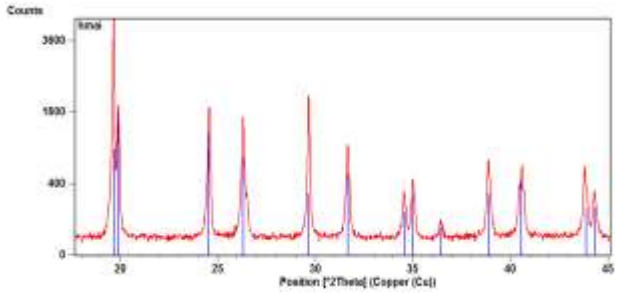

Fig. 6. XRD pattern of synthesized methylammonium iodide (MAI). Blue lines indicate the reference peak position of MAI.

Although, all the obtained peaks are assigned to the methylammonium iodide, the color of obtained powder was light yellow which means a small amount of residual reagents is still mixed with the ammonium salts or small amount of water vapor was observed as the salt is hygroscopic. In order to purify the salt, we wash the powders with diethyl ether at room temperature to remove the residues, as the diethyl ether is a good solvent for amine and the acid but the salts have very low solubility in it. After washing the salts several times, a white powder was obtained ratify the disposal of residual reagent and the elimination of the observed water vapor as confirmed by using FTIR for unwashed and washed powders, fig. 7 a and b.

The FTIR patterns show the band around 3400 cm^{-1} which attributed to N-H stretching and the band at 3100 cm^{-1} which corresponds to the vibrational stretching mode of the hydroxyl group O-H. The band observed around 1480 cm^{-1} corresponds to the symmetric NH3 bending while the bands around 1200 cm^{-1} and 800 cm^{-1} corresponds to the C-N stretching and NH3 stretching respectively. It is clear that, band at 3100cm^{-1} (O-H group) is reduced after washing as a result of eliminate water vapor absorbed by powder.

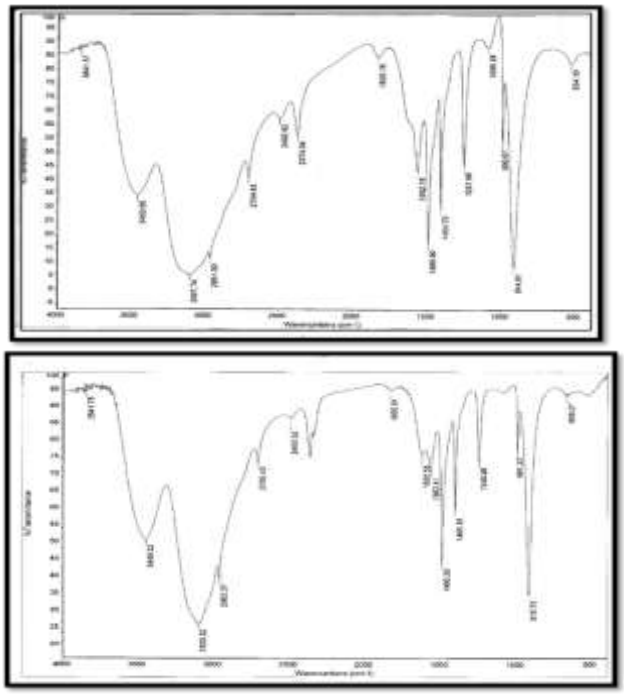

Fig. 7. The FTIR of MAI powders (a) unwashed sample, (b) washed sample

Fig. 8 shows the XRD pattern of the CH3NH3PbI3 layer based on FTO glass, synthesized at 100 ^oC using two step dipping method. A strong diffraction peaks at 14.14°, 20.05°, 23.53°, 24.53°, 28.50°, 31.95°, 40.54° and 43.11° are observed , which indicated to the tetragonal perovskite structure (space group: I 4 c m) with lattice parameters a = 8.85 Å and c = 12.63 Å. An additional peaks at 26.48, 33.74 and 37.80° are obtained and assigned to the (110), (101) and (200) planes of the tetragonal SnO2. In addition to the detected peaks, a peak at 12.66^o is detected, which belongs to unreacted PbI2.

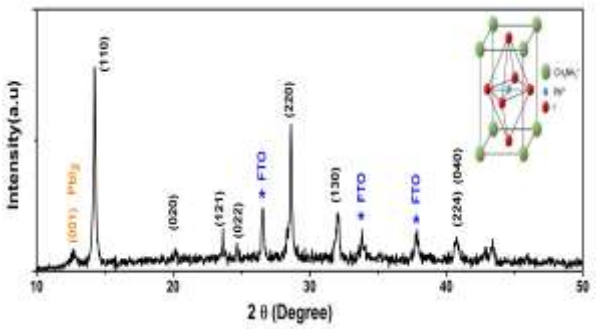

Fig. 8. XRD pattern for CH3NH3PbI3 based on TiO2 layers. Insert shows the Tetragonal system of perovskite structure.

B. Photovoltaic Characteristics of PSCs

In order to ensure the best method to fabricate the cell, three different methods were carried out using same materials under the same conditions. At each method, three devices were fabricated, each one contains 3 cells, and tested under the same conditions. The J-V curve of the best-performing devices for different methods are shown in fig. 9. The corresponding open-circuit potential (V_{oc}), short-current density (J_{sc}), Fill factor (FF) and PCEs, are summarized in table 2.

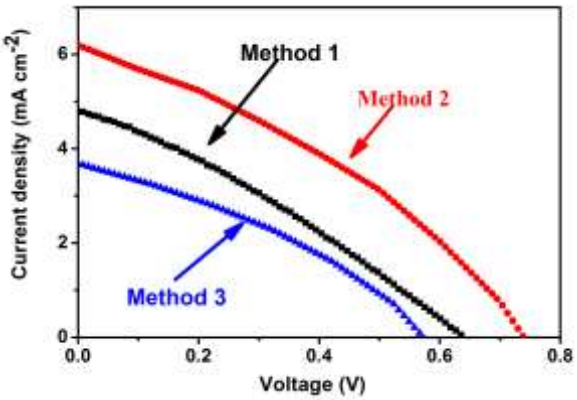

Fig. 9. J-V curves for the PSCs,

Table 2: Photovoltaic parameters of PSCs

	V_{oc} (V)	J_{sc} (mA)	F.F %	PCE %
Method 1	0.64	4.78	31	0.95
Method 2	0.74	6.19	34.2	1.57
Method 3	0.57	3.69	34.7	0.73

The results clearly indicate that the different methods of carbon layer deposition have a significant effect on the overall power conversion efficiency. Method 3 achieved the poorer photovoltaic performance (Voc of 0.56 V, Jsc of 3.69 mA cm-2, FF of 0.34, and PCE of 0.73%) as a result of the poor contact between the perovskite layer and the carbon layer via the mechanical joining (Sandwich process).

In method 1 (open cell), the V_{oc}, J_{sc}, and FF are improved to 0.64 V, 4.78 mA cm-2, and 0.31, respectively, yielding an enhanced PCE of 0.95%. The direct deposition of carbon layer on the perovskite layer facilitates their contact and hence minimize the electrical resistance, enhancing the device performance. In addition, this method is sustainable for large scale production compared with the sandwich device.

Method 2 showed the best cell performance compared to that of Method 1 and Method 3, with Voc of 0.74 V, Jsc of 6.19 mA cm-2, FF of 0.34, and PCE of 1.57%. The deposition of carbon above PbI2 layer, thereafter dipping in the MAI solution leading to in situ conversion of PbI2 to CH3NH3PbI3 and chemical embedding of C into CH3NH3PbI3 at the interface. The in situ conversion of PbI2 to CH3NH3PbI3 leads to greatly improve the interface and lower the barrier for facile hole extraction.

In order to investigate the reproducibility of the PSC devices using the different methods, fig. 10, shows the average photovoltaic parameters with their standard deviation. As can see, the average photovoltaic parameters based on method 1 and 2 are approximately close compared with method 3. Although method 2 have slightly higher average photovoltaic parameters than methods 1, it involving higher standard deviation.

The higher standard deviation might be attributed to: the formed perovskite layer has a variation in the particle size and therefore an enormous particle might leads to minify the CH3NH3PbI3 / C contact. Moreover, Method 2 required more precautions to avoid the short circuit during pasting the C layer above PbI2.

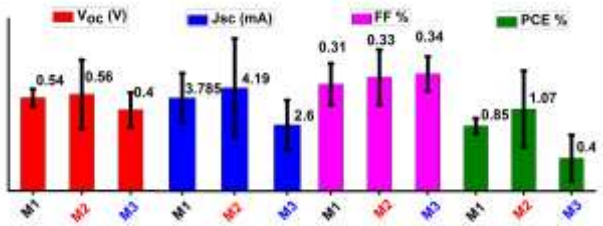

Fig. 10. Photovoltaic parameters for PSCs, fabricated by the three different methods

IV. CONCLUSION

Three different methods were applied for fabricating free-hole transport layer PSC devices, using Carbon as a counter electrode. In consideration of the same TiO2 and carbon layers used for the three methods, the direct deposition of carbon paste on CH3NH3PbI3 layer using Doctor Blading technique (Method 1) achieved best and non-varying (PCE of 0.95 %) photovoltaic performance compared with the other methods.

REFERENCES

[1] D. Bi, W. Tress, M.I. Dar, P. Gao, J. Luo, C. Renevier, K. Schenk, A. Abate, F. Giordano, J.P.C. Baena, J.D. Decoppet. "Efficient luminescent solar cells based on tailored mixed-cation perovskites." *Science Advances*, vol. 2, 2016.

[2] L. Huang, Z. Hu, J. Xu, K. Zhang, J. Zhang, Y. Zhu. "Multi-step slow annealing perovskite films for high performance planar perovskite solar cells." *Solar Energy Materials and Solar Cells*, vol. 141, pp. 377–382, 2015.

[3] H. Back, J. Kim, G. Kim, T.K. Kim, H. Kang, J. Kong, S.H. Lee, K. Lee. "Interfacial modification of hole transport layers for efficient large-area perovskite solar cells achieved via blade-coating." *Solar Energy Materials and Solar Cells*, vol. 144, pp. 309–315, 2016.

[4] J. Xing, X.F. Liu, Q. Zhang, S.T. Ha, Y.W. Yuan, C. Shen, T.C. Sum, Q. Xiong. "Vapor phase synthesis of organometal halide perovskite nanowires for tunable room temperature nano lasers." *Nano Letters*, vol. 15, pp. 4571–4577, 2015.

[5] K.F. Lin, S.H. Chang, K.H. Wang, H.M. Cheng, K.Y. Chiu, K.-M. Lee, S.H. Chen, C.G. Wu. "Unraveling the high performance of tri-iodide perovskite absorber based photovoltaics with a non-polar solvent washing treatment." *Solar Energy Materials and Solar Cells*, vol. 141, pp. 309–314, 2015.

[6] J.H. Heo, S.H. Im, J.H. Noh, T.N. Mandal, C.S. Lim, J.A. Chang, Y.H. Lee, H. J. Kim, A. Sarkar, M.K. Nazeeruddin, M. Grätzel, S.I. Seok. "Efficient inorganic– organic hybrid heterojunction solar cells containing perovskite compound and polymeric hole conductors." *Nature Photonics*, vol. 7, pp. 486-491, 2013.

[7] J. Burschka, N. Pellet, S.J. Moon, R. Humphry-Baker, P. Gao, M.K. Nazeeruddin, M. Gratzel. "Sequential deposition as a route to high-performance perovskite sensitized solar cells." *Nature*, vol. 499, pp. 316–319, 2013.

[8] Y. Zhao, A. M. Nardes, Kai Zh. "Solid-State Mesostructured Perovskite CH3NH3PbI3 Solar Cells: Charge Transport, Recombination, and Diffusion Length." *The Journal of Physical Chemistry Letters*, vol, 5, pp. 490-494, 2014.

[9] J. Xiao, J. J. Shi, D. M. Li and Q. B. Meng. "Perovskite thin-film solar cell: excitation in photovoltaic science." *Science China Chemistry*, vol. 58, pp. 221-238, 2015.

[10] Z. Zhu, J. Ma, Z. Wang, C. Mu, Z. Fan, L. Du, Y. Bai, L. Fan, H. Yan, D. L. Phillips, S. Yang. "Efficiency Enhancement of Perovskite Solar Cells through Fast Electron Extraction: The Role of Graphene Quantum Dots" *The Journal of the American Chemical Society*, vol. 136, pp. 3760 –3763, 2014.

[11] J. Qiu, Y. Qiu, K. Yan, M. Zhong, C. Mu, H. Yan, S. Yang. "All-solid-state hybrid solar cells based on a new organometal halideperovskite sensitizer and one-dimensional TiO2 nanowire arrays" *Nanoscale*, vol. 5, pp. 3245 – 3248, 2013.

[12] D. Li, Y. Chen, P. Du, Z. Zhao, H. Zhao, Y. Ma, Z. Sun." An annealing-free anatase TiO2 nanocrystal film as an electron collection layer in organic solar cells." *RSC Advances*, vol. 5, pp. 88973–88978, 2015.
[13] Y. Zhao, Q. Zeng, X. Liu, S. Jiao, G. Pang, X. Du, K. Zhang, B. Yang. "Highly efficient aqueous-processed polymer/nanocrystal hybrid solar cells with an aqueous-processed TiO2 electron extraction layer." *Journal of Materials Chemistry A*, vol. 4, pp. 11738–11746, 2016.
[14] K. Wojciechowski, M. Saliba, T. Leijtens, A. Abate and H. J. Snaith. "Sub-150 °C processed meso-superstructured perovskite solar cells with enhanced efficiency." *Energy & Environmental Science*, vol. 7, pp. 1142–1147, 2014.
[15] W. Yongzhen, A. Islam, X. Yang, C. Qin, J. Liu, K. Zhang, W. Peng, L. Han. "Retarding the crystallization of PbI2 for highly reproducible planar-structured perovskite solar cells via sequential deposition" *Energy & Environmental Science*, vol. 7, pp. 2934 – 2938, 2014.
[16] A. Yella, L. P. Heiniger, P. Gao, M. K. Nazeeruddin and M. Gratzel. " Nanocrystalline Rutile Electron Extraction Layer Enables Low-Temperature Solution Processed Perovskite Photovoltaics with 13.7% Efficiency." *Nano Letters*, vol. 14, pp. 2591–2596, 2014.
[17] J. A. Christians, R. C. Fung, P. V. Kama. "An Inorganic Hole Conductor for Organo-Lead Halide Perovskite Solar Cells. Improved Hole Conductivity with Copper Iodide" *Journal of the American Chemical Society*, vol. 136, pp. 758 – 764, 2014.
[18] S. Ye, W. Sun, Y. Li, W. Yan, H. Peng, Z. Bian, Z. Liu and C. Huang. "CuSCN - Based Inverted Planar Perovskite Solar Cell with an Average PCE of 15.6%." *Nano Letters*, vol. 15, pp. 3723–3728, 2015.
[19] Z. Ku, Y. Rong, M. Xu, T. Liu and H. Han. "Full printable processed mesoscopic $CH_3NH_3PbI_3/TiO_2$ heterojunction solar cells with carbon counter electrode. "*Scientific* Reports, vol. 3, pp. 3132–3137, 2013.
[20] Y. Rong, Z. Ku, A. Mei, T. Liu, M. Xu, S. Ko, X. Li and H. Han. "Hole-Conductor-Free Mesoscopic $TiO_2/CH_3NH_3PbI_3$ Heterojunction Solar Cells Based on Anatase Nanosheets and Carbon Counter Electrodes." *The Journal of Physical Chemistry Letters*. Vol. 5, pp. 2160–2164, 2014.
[21] W. A. Laban and L. Etgar. "Depleted hole conductor-free lead halide iodide heterojunction solar cells." *Energy & Environmental Science*, Vol. 6, pp. 3249–3253, 2013.
[22] L. Etgar, P. Gao, Z. Xue, Q. Peng, A. K. Chandiran, B. Liu, M. K. Nazeeruddin, M. Gratzel. "Mesoscopic CH3NH3PbI3/TiO2 Heterojunction Solar Cells." *The Journal of the American Chemical Society*, Vol. 134 (42), pp 17396–17399, 2012.
[23] P. Vivo, A. Ojanpera, J.H. Smått, S. Sanden, S. G. Hashmi, K. Kaunisto, P. Ihalainen, M. T. Masood, R. Osterbacka, P. D. Lund and H. Lemmetyinen. "Influence of TiO2 compact layer precursor on the performance of perovskite solar cells" *Organic Electronics*, vol. 41, pp. 287-293, 2017.
[24] L. Lutterotti, P. Scardi, P. Maistrelli. (1992) LSI—A Computer "Program for Simultaneous Refinement of Material Structure and Microstructure". *Journal of Applied Crystallography*, vol. **25**, 459-462.
[25] H.M.Rietveld. "Line profiles of neutron powder-diffraction peaks for structure refinement" *Acta Crystallographica*, vol. 22, pp. 151-152, 1967.